UCID- 17328

Lawrence Livermore Laboratory

A SOVIET PAPER ON LASER TARGET HEATING, SYMMETRY OF IRRADIATION, AND TWO-DIMENSIONAL EFFECTS ON COMPRESSION

Harry L. Sahlin

December 13, 1976

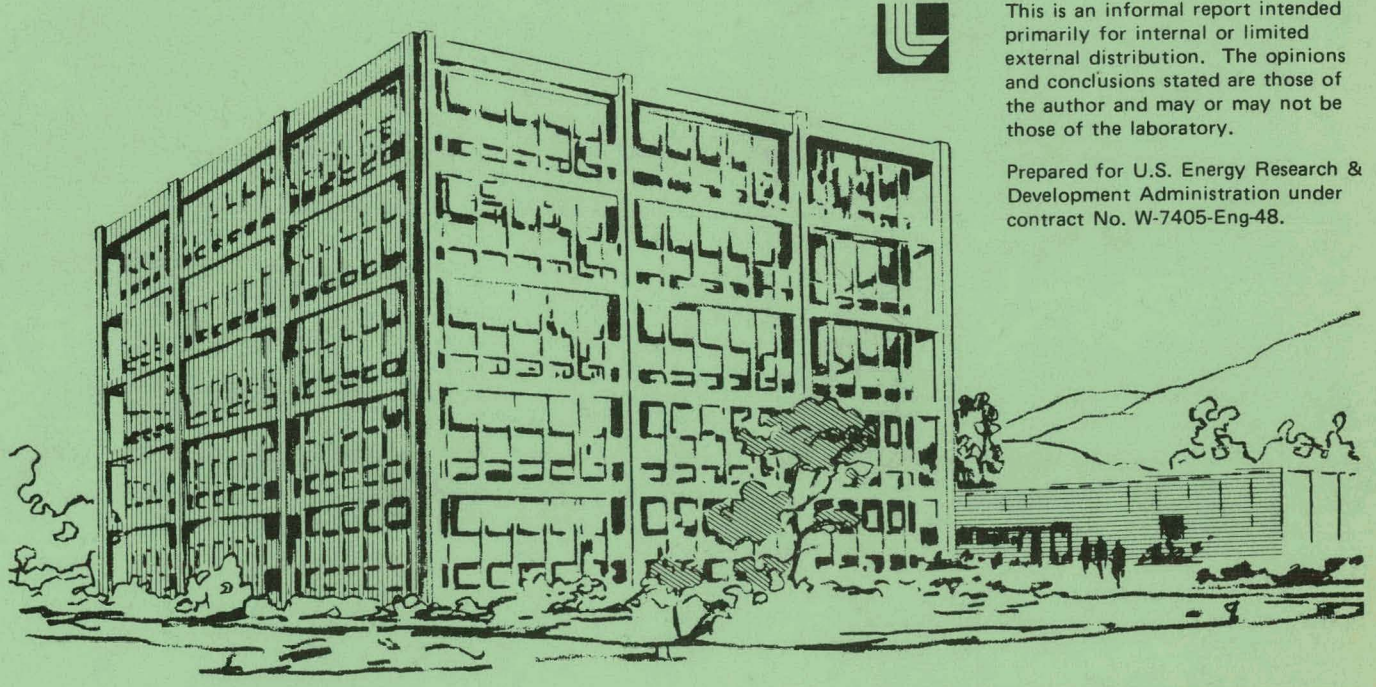

Prepared for U.S. Energy Research & Development Administration under contract No. W-7405-Eng-48.

DISCLAIMER

A SOVIET PAPER ON LASER TARGET HEATING, SYMMETRY OF IRRADIATION, AND TWO-DIMENSIONAL EFFECTS ON COMPRESSION

On Friday, November 19, 1976, Dr. Yu. V. Afanasiev (Lebedev Physical Institute, Moscow) presented a paper entitled "Theoretical Study of Laser Target Heating, Symmetry of Irradiation, and Two-Dimensional Effects on Compression" to a poorly attended post-deadline session of the Annual Meeting of the Plasma Physics Division of the American Physical Society in San Francisco. Because this report contains new and important information related to two-dimensional calculations for laser target compression, it deserves wider distribution.

Afanasiev et al. develop and use a one-dimensional self-consistent analytical model of the steady-state corona of a laser-irradiated slab target to obtain the efficiences of absorption of laser energy by the target and the percent reflected for various Nd-laser-pulse shapes in the range between 10^{12} and 10^{16} W/cm^2. These theoretical deductions are compared with the experiment. The model employs a δ-function-like energy absorption of the laser light at the critical surface. The symmetry of target irradiation from a multiple-beam system is considered and related to the specific case of the 216-channel 10-kJ Nd-glass installation named "Delfin" presently under construction in the Basov Laboratory at the Lebedev Institute. Two-dimensional calculations of laser-driven compression for a 70-μ radius, 4-μ-thick-walled glass microballon ($R/\Delta R = 17.5$) with a 100-J, 2-ns pulse for both the case of flux asymmetry and inhomogeneity are given. Both the case of large and small initial asymmetry are presented. Shell inhomogeneties less than 3% are found to be compatible with achievement of 1000-fold compression, while those greater than 10% lead to significant deviation of the final target shape from spherical symmetry.

This paper is related to the important and controversial earlier work by Afanasiev et al. on high-gain laser-driven pellets first published in JETP Letters 21, 68 (1975).

As a result of lasnex calculations by T. Buckholtz, J. Brandenberg, and myself at LLL, and by R. Freeman and J. Brownell at LASL, on laser-driven and plasma-focus-driven modified Russian targets, supplemented by some additional information gained in discussion with Dr. Afanasiev, it has been possible to virtually duplicate the yield, densities, and temperatures of the 10^{-3} -gm

target given in the reference above (122 MJ). Work is in progress on calculations of the other targets and will be reported subsequently.

Appendix A gives the paper presented at the APS meeting. I have prepared it from the text and slides provided by Dr. Afanasiev. Although I have occasionally made minor additions and changed certain articles of speech for increased clarity, I have tried to stick to the original text as closely as possible.

A few passages and figures were deleted in the original text, perhaps by Soviet censors, and these are so indicated.

APPENDIX A: THEORETICAL STUDY OF LASER TARGET HEATING, SYMMETRY OF IRRADIATION, AND TWO-DIMENSIONAL EFFECTS ON COMPRESSION

Yu. V. Afanasiev, N. G. Basov, E. G. Gamaly, N. N. Demchenko,
O. N. Krokhin, V. B. Rozanov, A. A. Samarsky, and A. P. Favorsky
Lebedev Physical Institute, Moscow

In this report we shall consider some theoretical problems of laser target irradiation and compression investigated at the laboratory of quantum radiophysics of Lebedev Physical Institute.

1. Of significant interest is the problem of absorption and reflection of laser radiation in the corona plasma of a laser target. Up to now there has been no satisfactory theoretical interpretation of numerous experiments on reflection and absorption. There is also no theoretical evidence for the formation of energy balance in the corona. These problems will be treated within the framework of a hydrodynamic description of the plasma corona.

Consider a plane self-consistent problem of the absorption and reflection of laser radiation in the expanding high-temperature plasma. Laser radiation transfer will be described by maxwellian equations. Let a monochromatic electromagnetic wave, $p = 0_o^{imZ}$, be incident on a plane plasma layer from $Z = -\infty$. The process of plasma heating and expansion is described by the group of equations in Fig. 1.

Figures 2 and 3 show the properties of plasma permittivity for a purely Coulomb ion-electron scattering and for the case of anomalous light absorption by plasma from the data obtained by the group of Dr. V. P. Silin at the Lebedev Institute.

As for the method of solution, note that it is convenient to introduce P and R functions, $V = R/P$, and then to get an equation for V by making use of the fact that in the region above critical density, where the field is absent, $V = 0$.

The model we discuss makes it possible to produce a physically correct self-consistent description of the absorption and reflection processes of monochromatic radiation by the plane-expanding plasma layer. Moreover, it

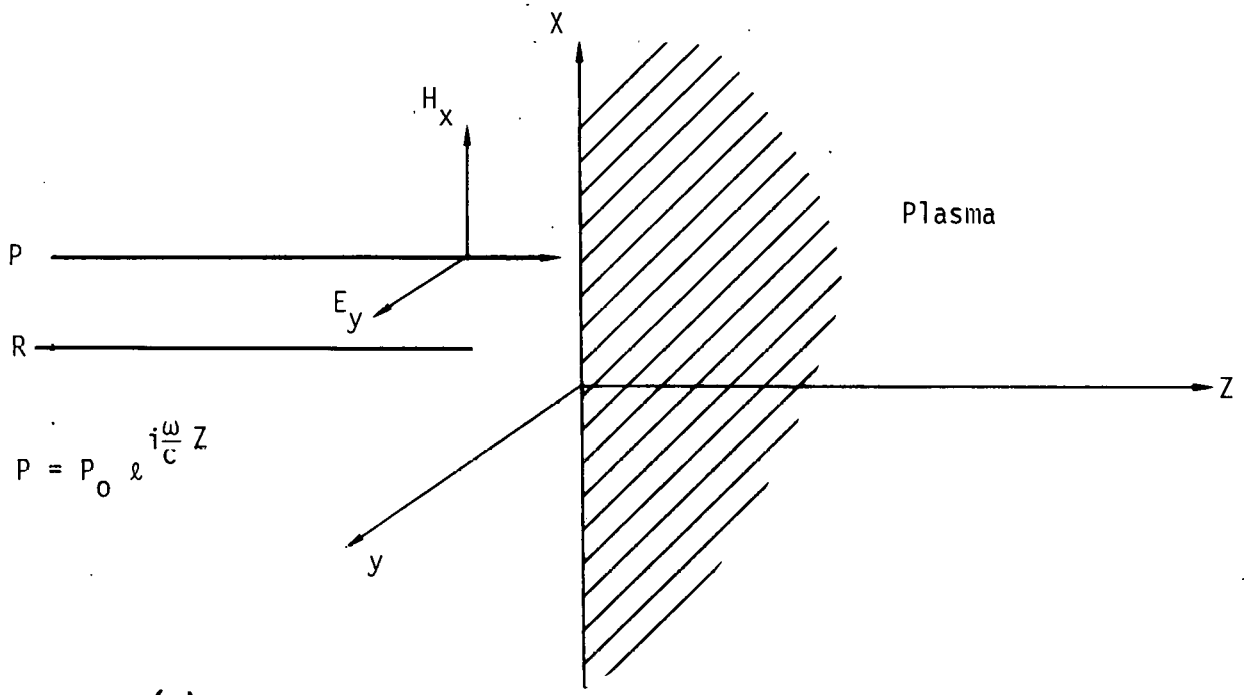

$$\frac{\partial}{\partial t}\left(\frac{1}{\rho}\right) = \frac{\partial u}{\partial m} \qquad \frac{\partial z}{\partial t} = u$$

$$\frac{\partial u}{\partial t} = - \frac{\partial}{\partial m}\left(p - \mu\rho\frac{\partial u}{\partial m}\right)$$

$$\frac{\partial \varepsilon_e}{\partial t} = - p_e \frac{\partial u}{\partial m} + \frac{\partial}{\partial m}\left(æ\rho\frac{\partial T}{\partial M}\right) + \frac{1}{\rho}\varepsilon_2\frac{\omega}{8\pi}|E_y|^2 - Q$$

$$\frac{\partial \varepsilon_i}{\partial t} = - \left(p_i - \mu\rho\frac{\partial u}{\partial m}\right)\frac{\partial u}{\partial m} + Q$$

$$\frac{\partial H_x}{\partial Z} + \frac{i\omega}{c}\varepsilon E_y = 0 \qquad \frac{\partial E_y}{\partial t} + \frac{i\omega}{c} H_x = 0$$

$$p_{e,i} = (\gamma - 1) A_{e,i} T_{e,i} \qquad \varepsilon_{e,i} = A_{e,i} T_{e,i}$$

$$\mu = \frac{4}{3}\eta_o T_i^{5/2}, \quad æ = æ_o T_e^{5/2}, \quad Q = Q_e \rho \frac{(T_e - T_i)}{T_e^{3/2}}$$

$$\varepsilon = \varepsilon_1 + i\,\varepsilon_2$$

Figure 1.

Permittivity for Coulomb ion-electron scattering

$$\varepsilon = \varepsilon_1 + i\,\varepsilon_2$$

$$\varepsilon_1 = 1 - a_o\,\rho$$

$$\varepsilon_2 = b_o\,\frac{\rho^2}{T_e^{3/2}}$$

Anomalous absorption

$$\varepsilon_2 = \frac{4\pi e^2\, n_e\, \nu_{eff}\,(n_e, T_e, Q_L)}{m_e \omega^3}$$

$$Q_L = \frac{c}{4\pi}\,|E|^2$$

Figure 2.

Given by Silin and Pustovalov

$$K\,(cm^{-1}) = 2\frac{\omega}{c}\left[\frac{1}{2}\left\{\sqrt{\left(1-\frac{\omega_p^2}{\omega^2+\nu_{eff}^2}\right)^2+\left(\frac{\nu_{eff}}{\omega}\,\frac{\omega_p^2}{\omega^2+\nu_{eff}^2}\right)^2}-1+\frac{\omega_p^2}{\omega^2+\nu_{eff}^2}\right]^{1/2}$$

Laser flux density Q	Electron density	ν_{eff}
$0 \leq Q \leq Q_o$	$0 \leq n_e \leq n_{cr}$	$\nu = \nu_0$
$Q_o \leq Q \leq \text{MIN}\,(Q_1,Q_2)$	$\left\lvert\left(\frac{n_e}{n_{cr}}\right)^{1/2}-1\right\rvert \leq \frac{3}{4}\left\{\ell n\,\frac{M_i}{Zm}\right\}^{-1}$	$\nu = \nu_1$
$Q_o \leq Q \leq \text{MIN}\,(Q_1,Q_2)$	$\left\{1-\left(\frac{n_e}{n_{cr}}\right)^{1/2}\right\} > \frac{3}{4}\left\{\ell n\,\frac{M_i}{Zm}\right\}^{-1}$	$\nu = \nu_0$
$\text{MIN}\,(Q_1,Q_2) \leq Q < \infty$	$\left\lvert\left(\frac{n_e}{n_{cr}}\right)^{1/2}-1\right\rvert < \left\{\frac{Zm}{M_i}\right\}^{1/2}$	$\nu = \nu_3$
$\text{MIN}\,(Q_1,Q_2) \leq Q < \infty$	$\left\{1-\left(\frac{n_e}{n_{cr}}\right)^{1/2}\right\} > 0{,}3$	$\nu = \nu_0$

$$Q_o = 5{,}4\cdot 10^{-18}\,Z^{3/2}\left(\frac{m}{M_i}\right)^{1/2} n_e^{3/2}\,T_e^{-1/2} \quad ; \quad Q_1 = 5{,}2\cdot 10^{15}\,T_e$$

$$Q_2 = Q_o\left(\frac{\nu_2}{\nu_o}\right)^2 \quad ; \quad \nu_o = 10^{-9}\,Z\,n_e\,T_e^{-3/2} \quad ; \quad \nu_1 = \nu_o\left(\frac{Q}{Q_o}\right)^{1/2}$$

$$\nu_2 = 5{,}65\cdot 10^4\,n_e^{1/2}\left(\frac{Zm}{M_i}\right)^{1/2} \quad ; \quad \nu_3 = 5{,}65\cdot 10^4\,n_e^{1/2}\left(\frac{Zm}{M_i}\right)^{1/3}$$

$$\left[Q\right]\ \frac{W}{cm^2} \quad ; \quad \left[T\right]\ keV$$

Figure 3.

$$E = P + R = P\,(1 + V) \quad , \quad V = \frac{R}{P}$$

$$H = \beta(-P + R) = \beta P(-1 + V)$$

$$\beta = \sqrt{\varepsilon} = \beta_1 + i\,\beta_2$$

$$\beta_1 = \sqrt{\frac{1}{2}\,(\varepsilon_1^2 + \varepsilon_2^2)^{1/2} + \frac{\varepsilon_1}{2}} \qquad \beta_2 = \sqrt{\frac{1}{2}\,(\varepsilon_1^2 + \varepsilon_2)^{1/2} - \frac{\varepsilon_1}{2}}$$

$$\frac{dP}{dZ} = \frac{i\omega}{c}\,\beta P - \frac{1}{2\beta}\,\frac{d\beta}{dZ}\left[P(1 - V)\right]$$

$$\frac{dV}{dZ} = -\,2\,\frac{i\omega}{c}\,\beta V + \frac{1}{2\beta}\,\frac{d\beta}{dZ}\,(1 - V^2)$$

$$V\,(Z_2) = 0 \qquad Z_2 > Z_{cr}$$

$$Q_L = \frac{c}{8\pi}\,|P|^2\left[\beta_1(1 - |V|^2) + 2\,\beta_2\,\mathrm{Im}\,V\right]$$

Figure 4.

enables us to interpret such important problems as the efficiency of light-energy contribution to plasma, spatial structure of the radiation field, and consequently, the structure of energy input, formation of the reflected wave, and time evolution of the reflection coefficient depending on the pulse and target parameters, particularly on the prepulse shape.

The results are reported for the Nd-glass laser ($\omega = 1.8 \times 10^{15} s^{-1}$) in the range of flux densities from 10^{12} to 10^{16} W/cm^2 for the plane DT-ice and $(CH_2)_n$-polyethylene targets, which are homogeneous at the beginning of the pulse.

Figure 5 shows the dependence of the integral coefficient of reflection $R = {}_0\int^t q^- dt / {}_0\int^t q^+ dt$ on the incident flux q^+ for the DT-layer with initial density 0.2 g/cm^2. Curve 1 corresponds to a classical absorption; curve 2, to anomalous absorption.

As seen from the diagram, the anomalous absorption plays an important role at flux densities above 10^{13} W/cm^2; the basic processes are the decay of light wave to the Langmuir oscillation and the ion sound.

Note that Fig. 5 illustrates the comparison of anomalous and classic absorptions. An increase in reflection with q^+ is associated with the dependence of the upper limit integration, $t = t(qt)$, equal to the time of layer bleaching, and decreases with an increase in the flux.

Figure 6 demonstrates the trajectories of the motion of DT-plasma critical density at various fluxes. We assume an anomalous mechanism of absorption.

Curves $q^+(t)$ illustrate the efficiency of energy contribution to DT plasma, which depends on the radiation flux and pulse duration with allowance for anomalous absorption. From the curves, it is seen that at any value of flux density the fraction of reflected energy decreases with increasing pulse duration, τ. This is due to the increase in time of the plasma layer optical thickness, kdz, and to the decrease in the reflection coefficient, $V(t)^2$. By changing the value of flux, the reflection can increase or decrease, depending on the pulse duration.

Figure 8 shows the profiles of density, temperature, and energy input per unit mass for the moment of time t = 1 ns after the action of laser radiation of 10^{14} W/cm^2. Note a sharp maximum of energy input near the

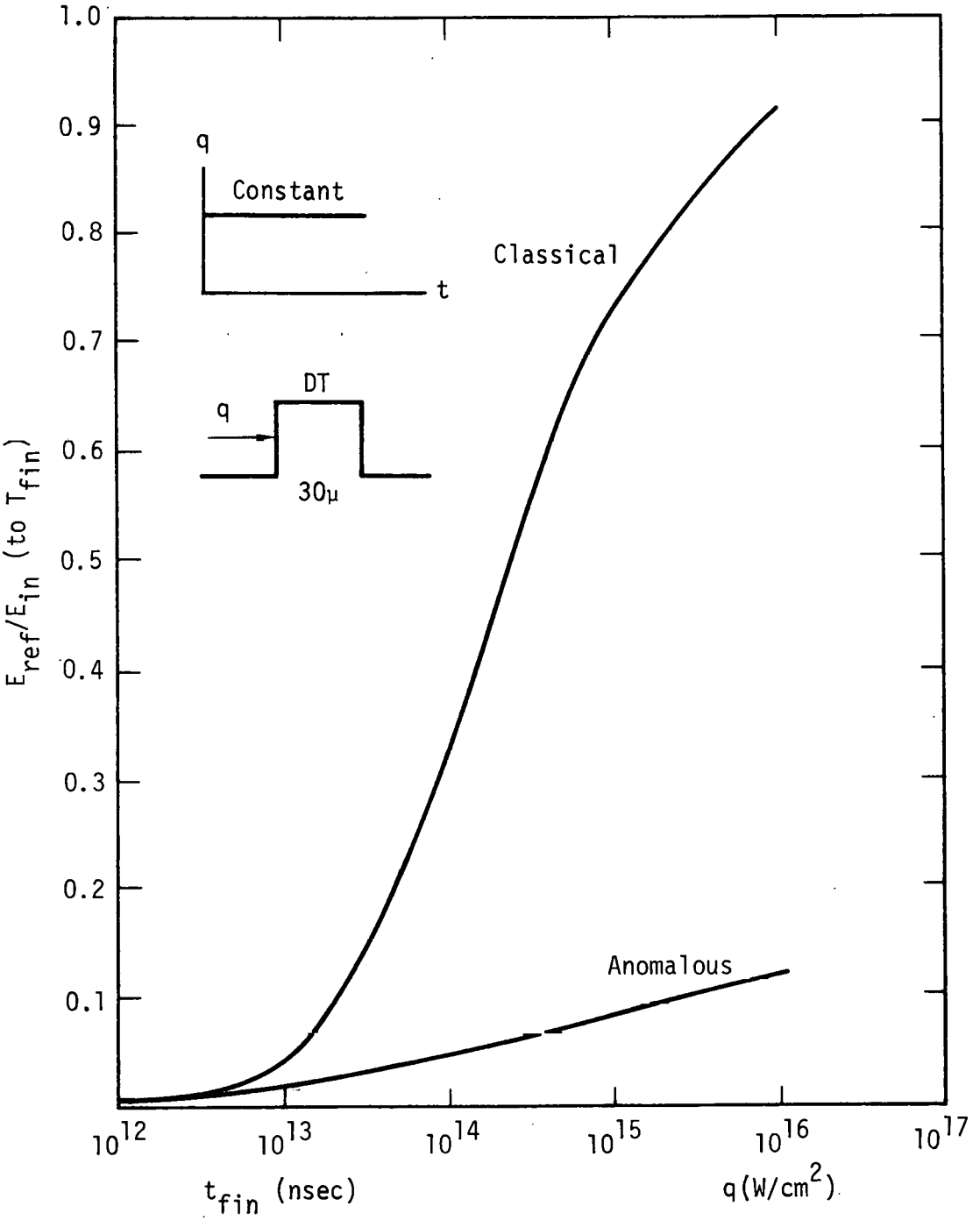

an	52	9.1	1.86	0.818	0.403
cl	52	9.3	2.35	1.35	0.881

Figure 5.

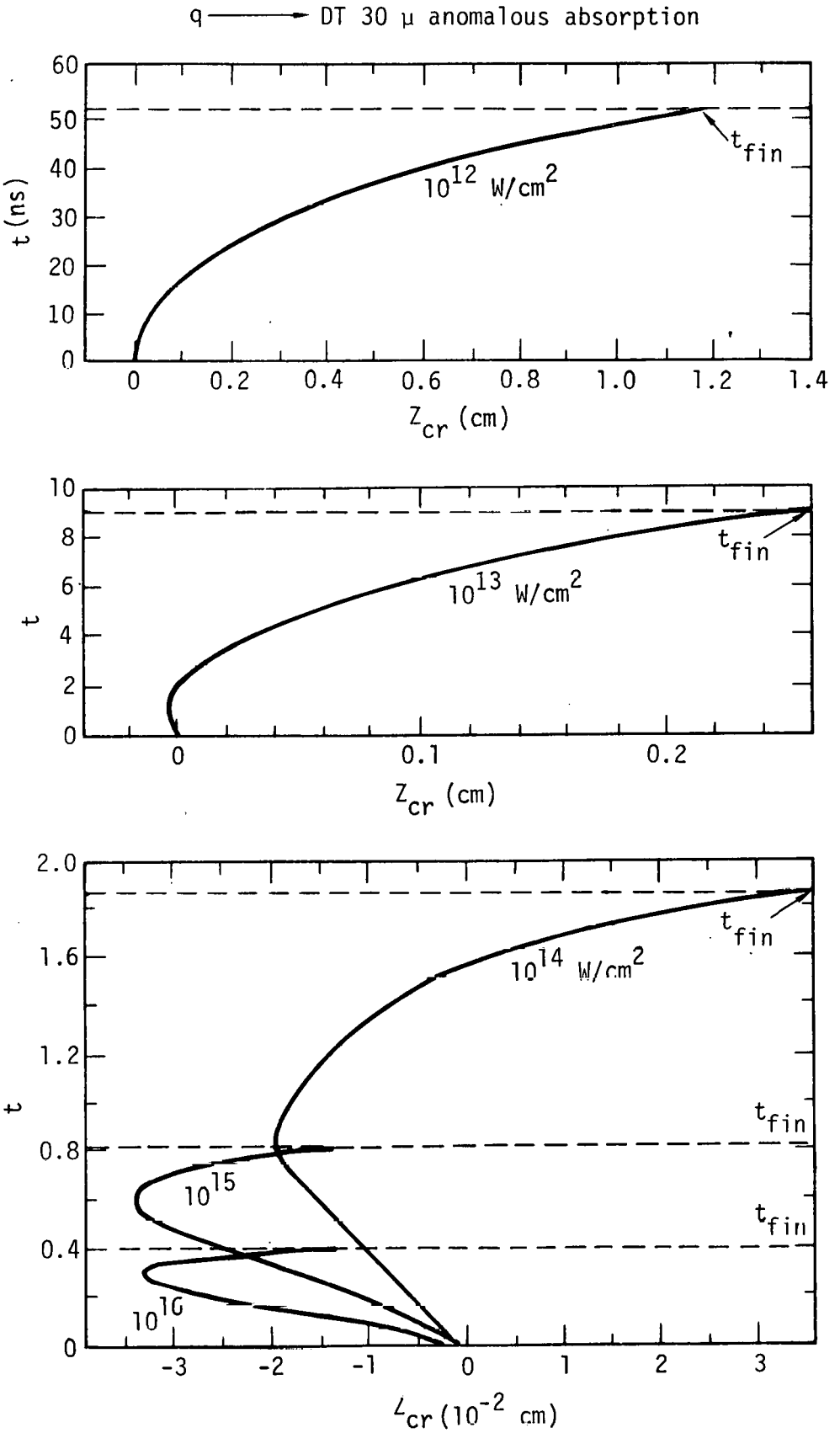
q ⟶ DT 30 μ anomalous absorption
t (ns)
10^{12} W/cm^2
t_{fin}
Z_{cr} (cm)
t
10^{13} W/cm^2
t_{fin}
Z_{cr} (cm)
t
10^{14} W/cm^2
t_{fin}
10^{15}
t_{fin}
10^{16}
Z_{cr} (10^{-2} cm)

Figure 6.

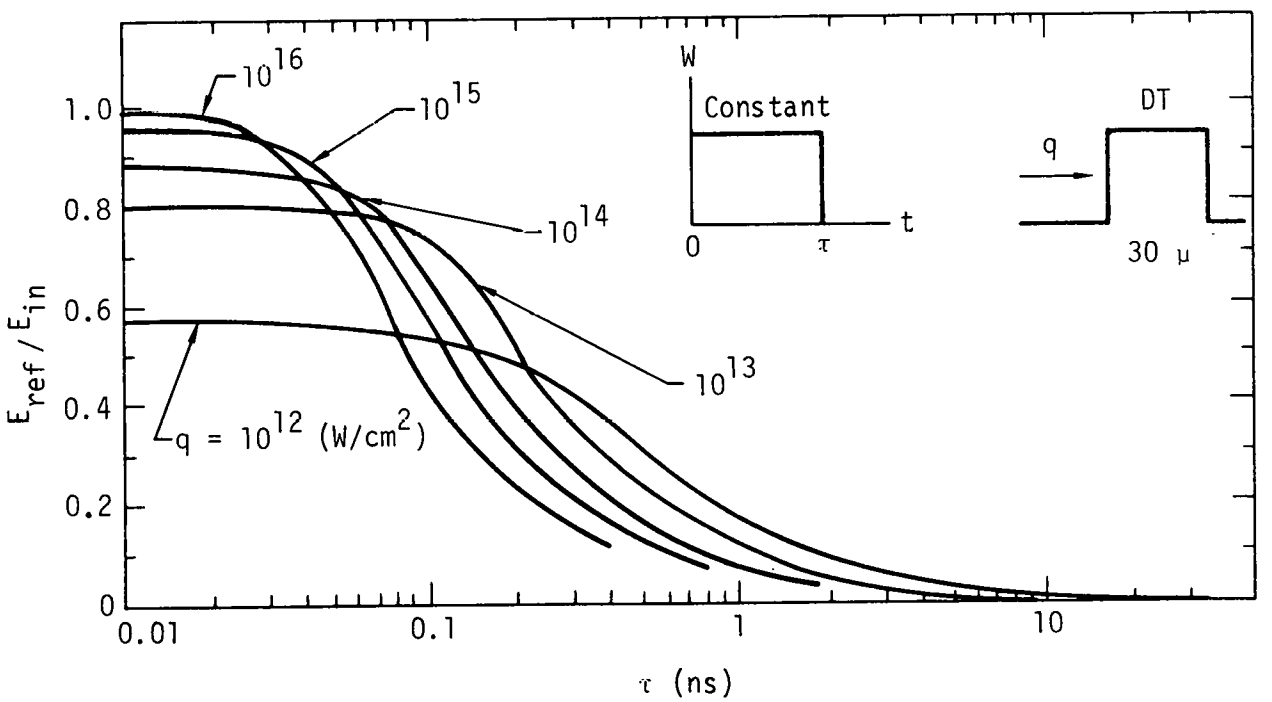
10^{16}
10^{15}
10^{14}
10^{13}
$q = 10^{12}$ (W/cm^2)
W
Constant
0
τ
t
DT
q
30 μ
E_{ref} / E_{in}
1.0
0.8
0.6
0.4
0.2
0
0.01
0.1
1
10
τ (ns)

Figure 7.

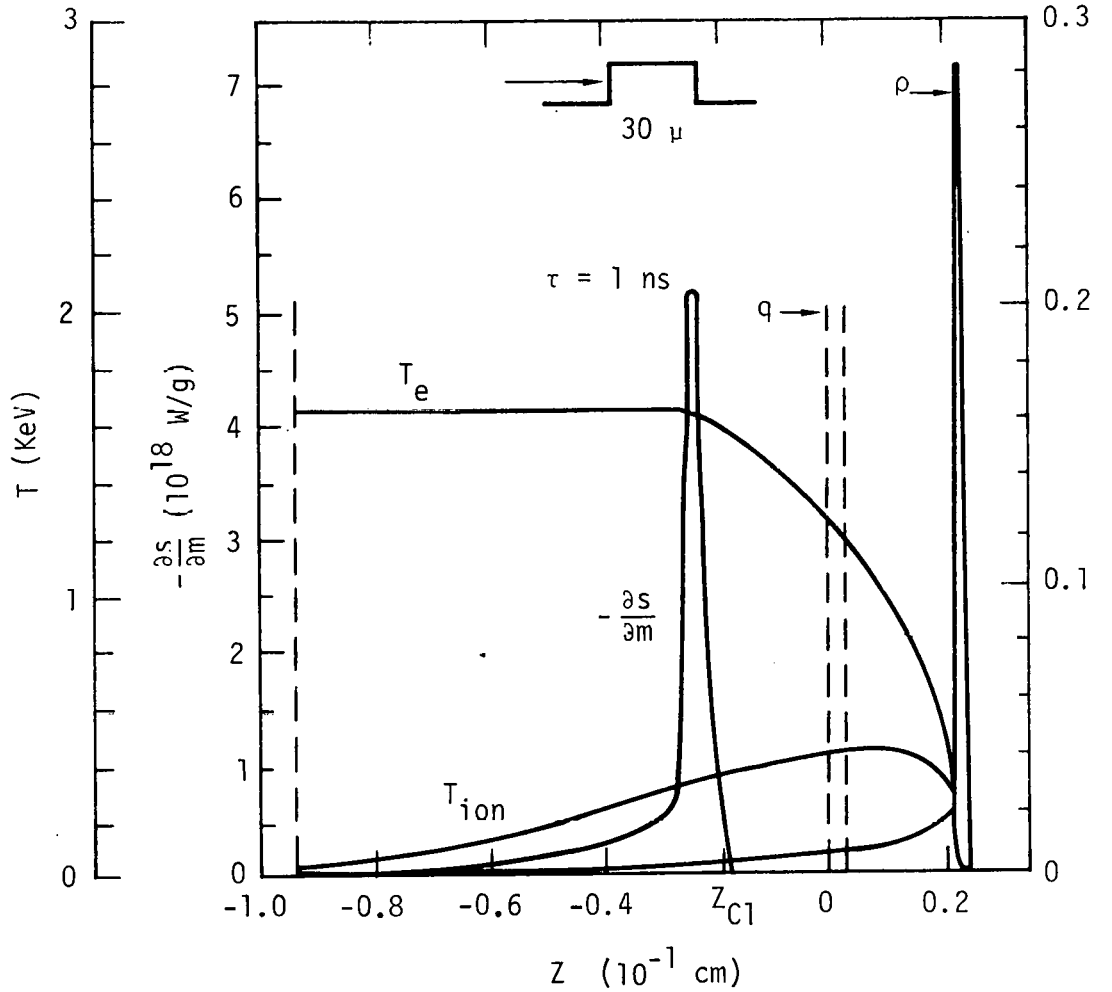
30 μ
ρ
τ = 1 ns
q
T_e
T_{ion}
$-\frac{\partial s}{\partial m}$
$-\frac{\partial s}{\partial m}$ (10^{18} W/g)
T (KeV)
$\rho\left(\frac{2}{cm^3}\right)$
Z_{Cl}
Z (10^{-1} cm)

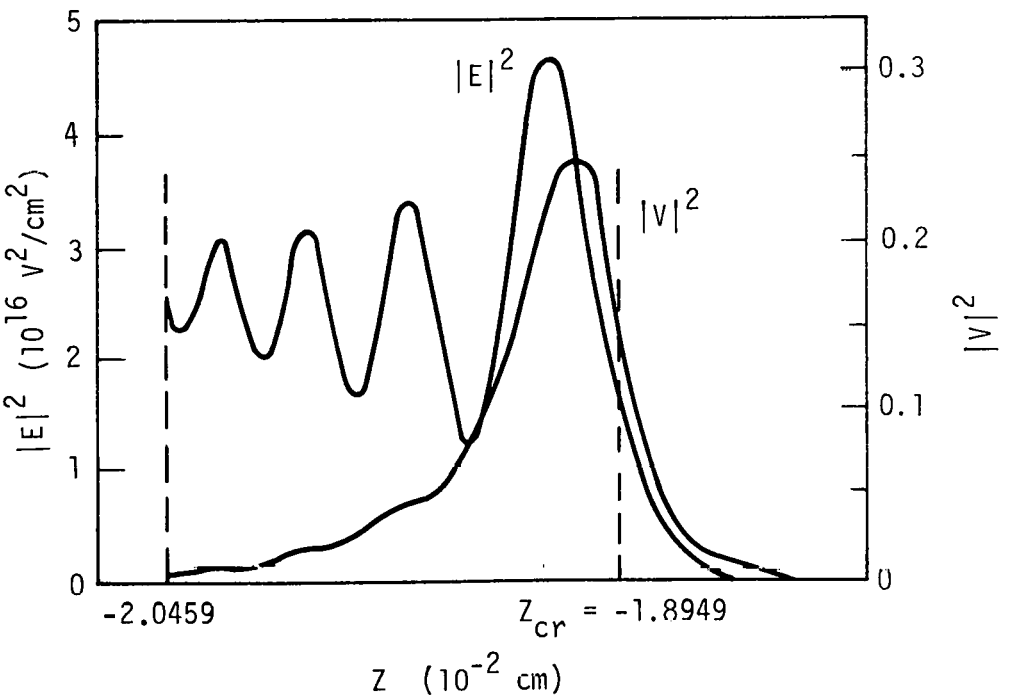
$|E|^2$
$|V|^2$
$|E|^2$ (10^{16} V^2/cm^2)
$|V|^2$
-2.0459
Z_{cr} = -1.8949
Z (10^{-2} cm)

Figure 8.

critical point connected with the anomalous absorption mechanism. The same figure illustrates the field structure $|E|^2$ and value $|E'|^2$ near the critical point.

Figure 9 shows the calculated results for conditions close to experimental for the reflection of a 4.75-ns-long laser pulse at flux densities 6.10^{13} W/cm^2 from the plane polyethylene $(CH_2)_n$ layer. The incident and reflected pulses are represented as well as the time dependence of value $|V|^2$, which corresponds to the instantaneous value for the reflection coefficient. The calculated fraction of reflected energy ($\sim$ 3.3%) agrees well with the experimental value of $\sim$ 3%. It should be noted that the interpretation of experiments with the plane targets in terms of the one-dimensional model has a qualitative character because the size of a focal spot is normally less than the dimension of the laser plasma. In the given case, the size of the laser plasma is about 100 μ, whereas that of the focal spot is 50 μ.

Finally, Fig. 10 illustrates the influence of the laser pulse contrast ratio on the value of reflected energy. A study is made of the rectangular 1.7-ns pulse with intensity of 10^{14} W/cm^2 and of the same pulse with a 3-ns-long prepulse, whose intensity increases linearly from zero to 10^{11} W/cm^2 (energy contrast $\sim 10^{-3}$). The reflected energy is 4.9% and 1.1%, respectively. A negligible prepulse energy changes the reflected energy by several times. From the reported calculations, it follows that the fraction of reflected energy may be significantly different, depending on the amount of flux, shape, and duration of the laser pulse. Because of anomalous absorption processes, the reflection coefficient in the range of fluxes up to 10^{15} W/cm^2 and pulse duration more than 1 ns is small and amounts to several percent. When comparing and interpreting the experimental data connected with measurement of the light-energy contribution to plasma, we should take into account a number of effects, such as the refraction of light and nonnormal incidence, which is not considered in our calculations.

2. The reported results make it possible to consider the problem of steady-state motion of the substance at spherically symmetric irradiation of a target with R_0 radius with the laser radiation flux Q_0. Stationary flow is established at the expense of spherical expansion of the expanding substance. The problem is based upon the assumption that laser energy is

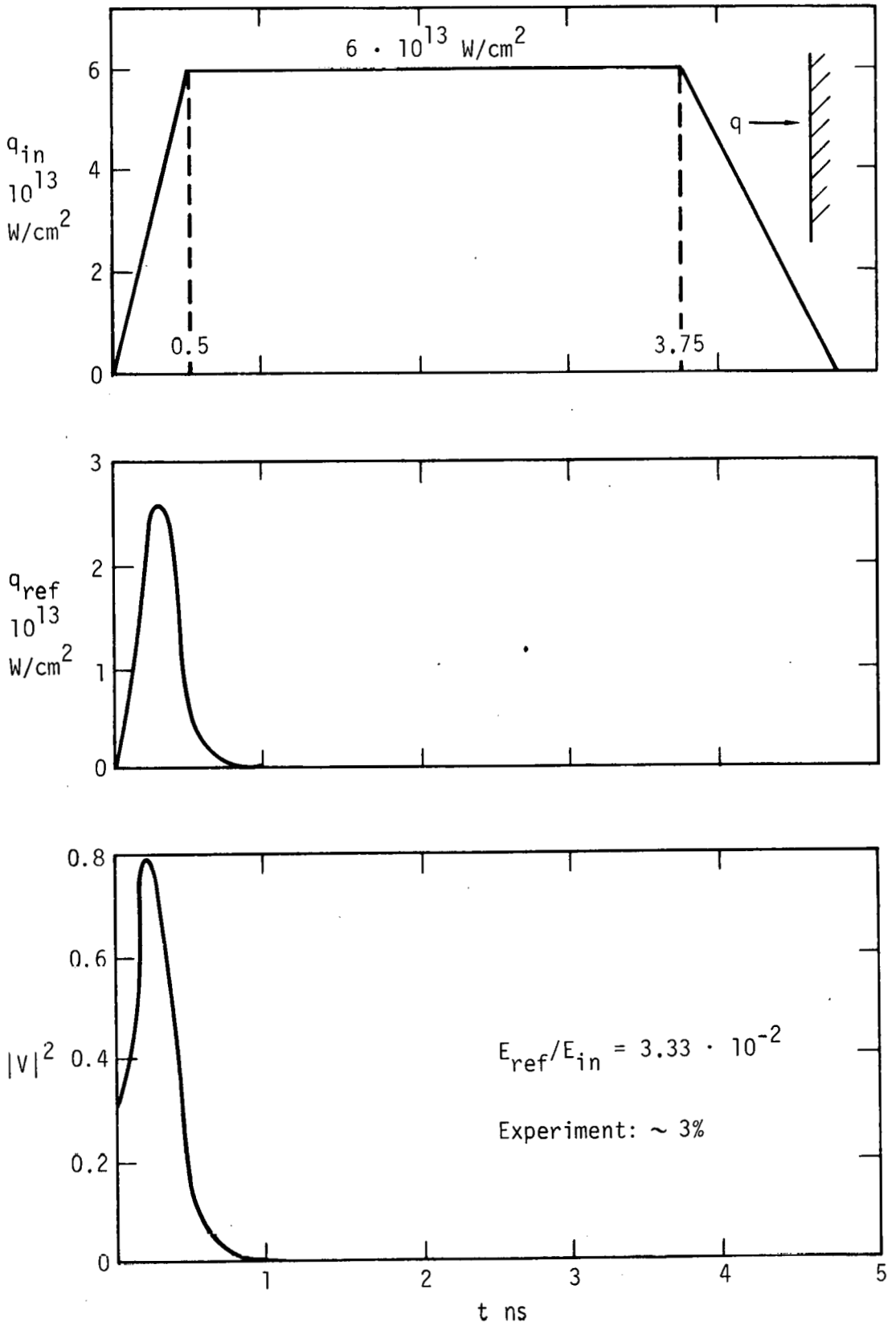
$6 \cdot 10^{13}$ W/cm^2
q_{in} 10^{13} W/cm^2
q
0.5
3.75
q_{ref} 10^{13} W/cm^2
$|V|^2$
$E_{ref}/E_{in} = 3.33 \cdot 10^{-2}$
Experiment: ~ 3%
t ns

Figure 9.

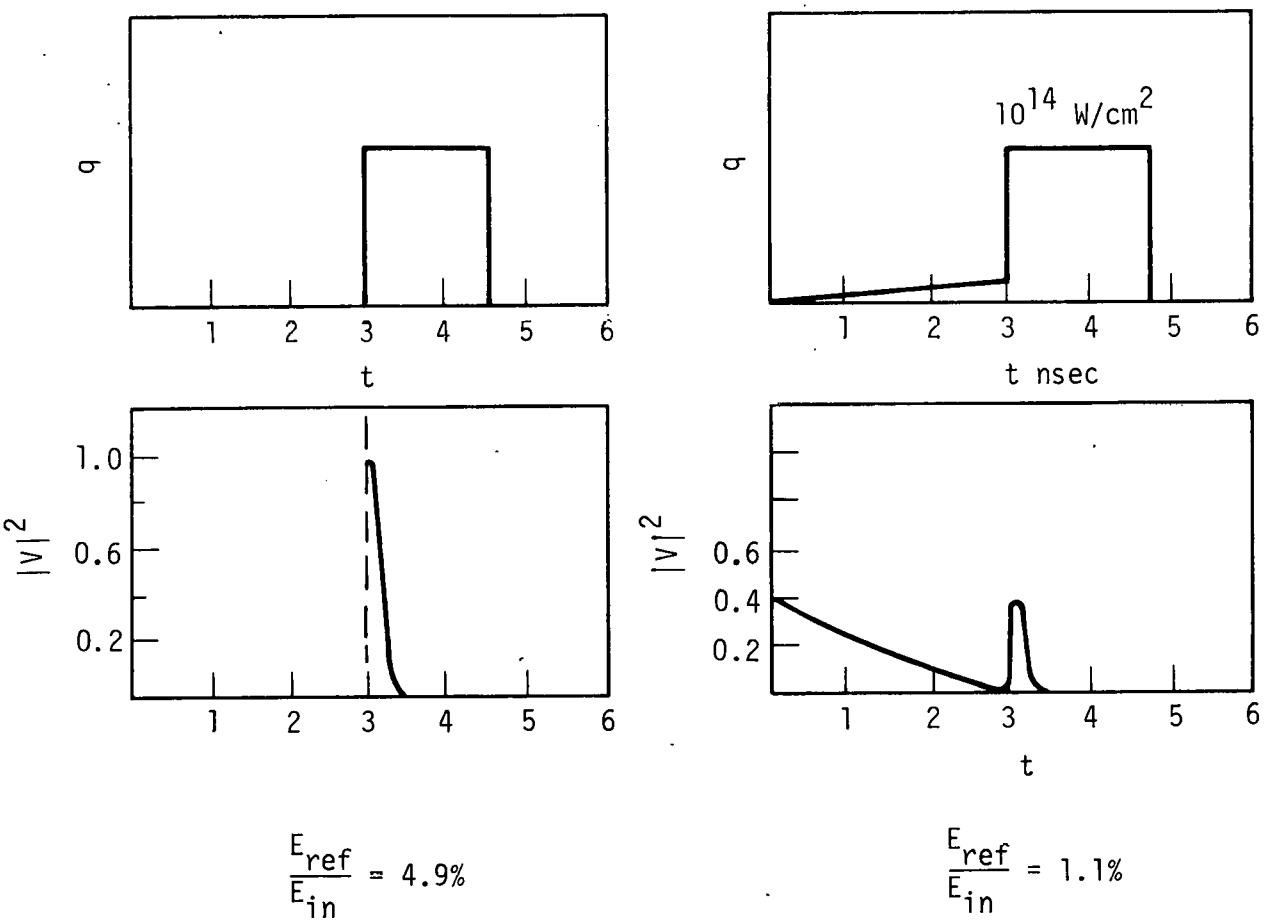

$\frac{E_{ref}}{E_{in}} = 4.9\%$

$\frac{E_{ref}}{E_{in}} = 1.1\%$

Figure 10.

absorbed near the critical density in a narrow zone. Hence, the energy input has a character of δ-function, as shown in Fig. 8. In addition, it is assumed that the absorbed laser energy is processed in the fluxes of electron-heat conductivity described in the Spitzer approximation.

Heat fluxes are directed from the critical zone to and from the target center. Equations of the problem and the corresponding boundary conditions are shown in Fig. 11.

Solution of the problem depends on the dimensionless parameter

$$\gamma_0 = \frac{\kappa_0^{3/4} Q_0}{\rho_{cr}^{1/4} R_0^{11/4}} \left(\frac{M_i}{Z+1}\right)^{21/8},$$

which includes the coefficient of electron heat conductivity κ_0, laser flux Q_0, critical density ρ_{cr}, target radius R_0, and mass and charge of the ion, M_i and Z. In the case of large value $\gamma_0 > 10^2$ (this case corresponds to large Q_0 and small R_0), the integral curves are represented in Fig. 12.

To find a solution, it is necessary to use the conditions for the curves transmitting a particular sonic point, where the sound velocity is equal to the velocity of flow. At the critical point $R = R_{cr}$, where $\rho = \rho_{cr}$, the temperature is maximal, the gasdynamic values are constant, and their derivatives discontinuous. The dependences of basic gasdynamic values of velocity, critical radius, and maximum temperature are represented in the figure by the formulas. With increase in the value of flux Q_0 (or decrease in the target radius R_0, or radiation frequency $\omega_{cr} \sim \rho_{cr}^{1/2}$), the radius of the critical point shifts toward the incident radiation, while the sonic point coordinate remains constant ($R_J = 1.2\ R_0$). In the case of small values of $\gamma \leq 5$ (small values of Q_0, large R_0 and ρ_{cr}), the radii of the critical and sonic points coincide; at further decrease of $\gamma_0 < 5$, they are driven toward the target surface. Integral curves for this case are shown in Fig. 12. A physically reasonable solution at $\gamma_0 < 5$ in the case of δ-shaped energy input can be built only under the condition that at the Jouhuet point the rate derivative turns to infinity, $\frac{dv}{dR} = \infty$. The figure shows the dependences of various gasdynamic values for the studied case of small fluxes.

The investigated stationary gasdynamic model of the laser target corona makes it possible to predict a number of physical values and compare them with the experiment. To make such a comparison valid, it is necessary

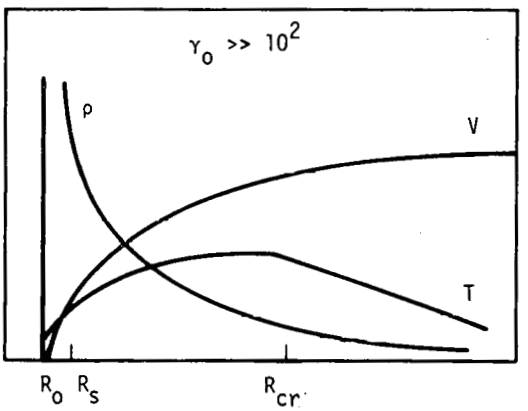

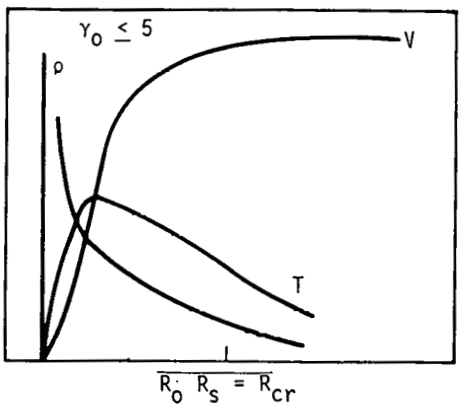

$$R_s = 1.2\, R_o$$

$$\rho_s \sim \frac{Q_o^{1/2}\, æ_o^{3/8}\, \rho_{cr}^{1/2}}{R_o^{7/8}} \left(\frac{M_i}{Z+1}\right)^{21/16}$$

$$v_s^2 \sim T_s \frac{Q_o^{1/3}}{æ_o^{1/4}\, \rho_{cr}^{1/12}\, R_o^{5/12}} \left(\frac{Z+1}{M_i}\right)^{7/8}$$

$$R_{cr} \sim R_o\, \gamma_o^{1/4}$$

$$v_{cr}^2 \sim v_s^2\, \ln \gamma_o \; ; \; T_{cr} \simeq 2.2\, T_s$$

$$v_\infty^2 \simeq \left[11 + 2 \ln \gamma_o\right] \cdot v_s^2$$

$$\gamma_o = \frac{Q_o\, æ_o^{3/4}}{\rho_{cr}^{3/4}\, R_o^{11/4}} \left(\frac{M_i}{Z+1}\right)^{21/8}$$

$$R_s = R_{cr} \simeq 1 + 0.022\, \gamma_o^{4/3}$$

$$\rho_s = \rho_{cr}$$

$$v_s^2 = v_{cr}^2 \sim T_s = T_{cr} \sim \left(\frac{Q_o}{R_{cr}\, R_o^2}\right)^{2/3}$$

$$v_\infty^2 \simeq (2.8)^2 \cdot v_s^2$$

Condition of stationary flow

$$\tau_{laser} > \frac{R_{cr}}{V_{cr}} = \begin{cases} \dfrac{Q_o^{0.08}\, R_o^{0.52}\, æ_o^{0.31}}{\rho_{cr}^{0.4}} \left(\dfrac{M_i}{Z+1}\right)^{1.1} & \gamma_o > 10^2 \\ R_o^{5/3} \left(\dfrac{\rho_{cr}}{Q_o}\right)^{1/3} & \gamma_o < 5 \end{cases}$$

Figure 11.

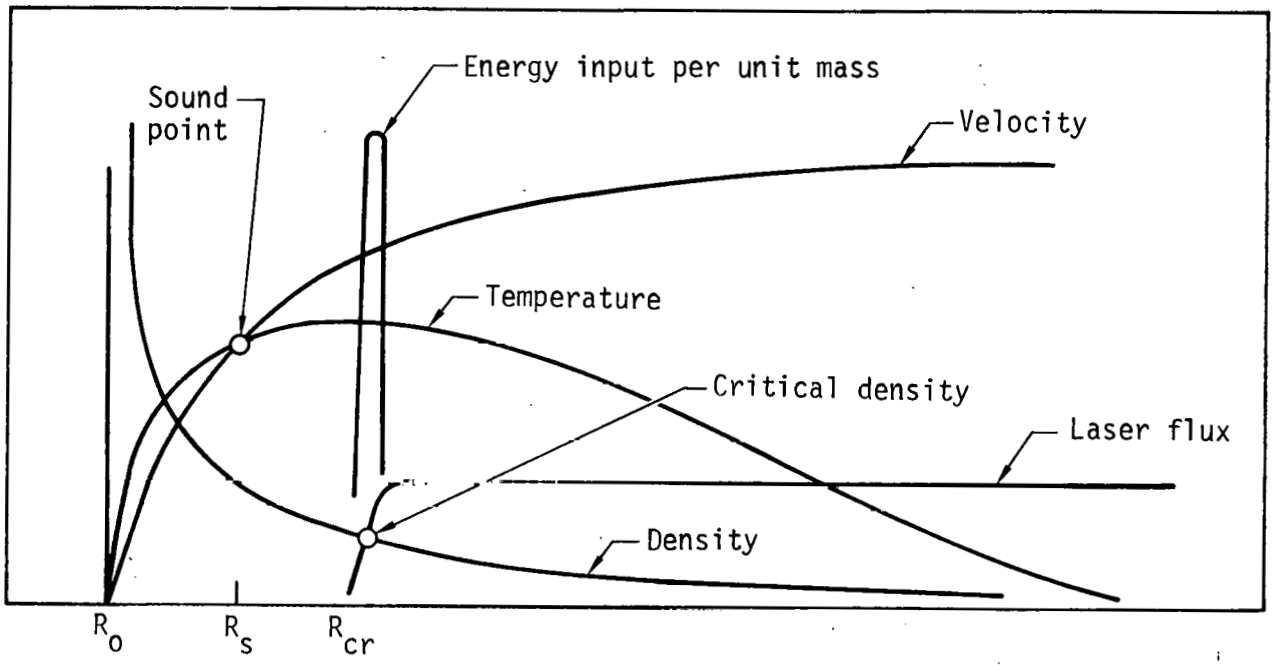

$$\rho v R^2 = \rho^* v^* R^{*2} = \text{Constant}$$

$$\frac{d}{dR}\left[P + \rho v^2\right] = -\frac{2\rho v^2}{R}$$

$$\rho v \cdot R^2 \left[\varepsilon + \frac{v^2}{2} + \frac{P}{\rho}\right] - R^2 \kappa_o T^{5/2} \frac{dT}{dR} =$$

$$= \begin{cases} Q_o & R > R_{cr} \\ 0 & R < R_{cr} \end{cases}$$

$$v(R_o) = T(R_o) = 0 \qquad T(\infty) = 0$$

$$p = \frac{Z+1}{M_i}\rho T \qquad c = \frac{1}{\gamma - 1}\frac{p}{\rho}$$

$$\gamma_o = \frac{\kappa_o^{3/4} Q_o}{\rho_{cr}^{7/4} R_o^{11/4}} \cdot \left(\frac{M_i}{Z+1}\right)^{21/8} \qquad \rho_{cr} = \frac{\omega_o^2 M_i m}{4\pi (Z+1) e^2}$$

Figure 12.

for the substance-flow around the target to have time to stabilize, i.e. that the laser pulse be sufficiently prolonged.

The quasistationary condition is τ pulse $> \frac{R_{cr}}{v}$. Throughout the development of this model of the corona, we should include the generation of fast ions; but in a purely gasdynamic description the fluxes must be moderate, and fast ions do not play a significant role in the energy balance. Figure 13 illustrates a number of calculated physical values, such as the outflow rate, maximum temperature, position of the critical point radius, and maximum pressure in the corona. Besides, some experimental values are shown, namely, temperature, pressure, and velocity of corona. There is satisfactory agreement between them. However, the present experiments do not contain sufficient data for the interpretation.

Of significant interest is a conclusion from the model under consideration that the target corona and hence the process of compression depend on the complex action of such values as flux, radiation frequency, material and radius of the target, and heat conductivity of plasma. If, for instance, the laser plasma heat conductivity is less or more than the predicted value, one can change experimental conditions to obtain the desirable characteristics of the corona.

3. Consider the problem of symmetry and homogeneity of spherical target irradiation by means of multi-channel arrangements with a great number of laser beams. If we separate all the beams of the arrangement into groups, which correspond to the number of edges in regular polyhedrons (N = 4,6,8,12,20), and then distribute them onto edges so as to preserve the symmetry of edge rotation, then it is sufficient to calculate the illuminance of a small ABC triangle. Illuminance of the whole target may be constructed for the reasons of symmetry. Our calculations are made on the assumption of an ideal optic and with allowance for small spherical aberrations.

Figure 14 [missing] shows a mean-statistic light distribution in the beam used in the calculations, geometry of sphere illumination by a single beam in the case of ideal optics, and expression for sphere illuminance by a single ideal beam. To allow for the spherical aberration, it should be noted that the focal distance depends on the distance of the beam to its optical axis. All installation beams are separated as N × M × L, where L is the number of beams in each group, M is the number of illuminating groups, and N is the number

$$\gamma_o = 0.46 \cdot 10^{-12} \left(\frac{A}{Z+1}\right)^{7/8} \left(\frac{10^{15}}{\omega}\right)^{7/2} R_o^{-3/4}\, Z^{-3/4}\, q_o$$

$\gamma_o \gg 10^2$

$$R_{cr}/R_o = 0.5\, \gamma_o^{2/7} \left[1 + 6.4\, \ell n \frac{\gamma_o^{2/7}}{4}\right]^{-1/4}$$

$$T_{cr} = 0.56 \cdot 10^{-10} \frac{A}{Z+1}\, \gamma_o^{-8/21} \left(\frac{q_o}{q_{cr}}\right)^{2/3}$$

$$p = 4.4 \cdot 10^{-3}\, \gamma_o^{4/21}\, \rho_{cr} \left(\frac{q_o}{\rho_{cr}}\right)^{2/3}$$

$$V_\infty^2 = 0.26 \cdot 10^5\, \gamma_o^{-8/21} \left[11 + 6.4\, \ell n \frac{\gamma_o^{2/7}}{4}\right] \left(\frac{q_o}{\rho_{cr}}\right)^{2/3}$$

$\gamma_o \lesssim 5$

$$R_{cr} = R_o\, V_{cr}^2 = 2.2 \cdot 10^4 \left(\frac{q_o}{\rho_{cr}}\right) \left[1 + 3 \cdot 10^{-2}\, \gamma_o^{4/3}\right]^{-4/3}$$

$$T_{cr} = 10^{-15} \frac{A}{Z+1}\, V_{cr}^2$$

$$p = 10^{-6}\, \rho_{cr}\, V_{cr}^2$$

$$V_\infty^2 = 8\, V_{cr}^2$$

$$T - \left[\text{keV}\right],\ V - \left[\frac{\text{cm}}{\text{sec}}\right],\ p - \left[\text{atm}\right],\ q_o - \left[\frac{\text{W}}{\text{cm}^2}\right]$$

	$R_o \mu$	$q_o \frac{W}{cm^2}$	τ nsec	R_{cr}/R_o	T_e^{cr} keV	P_{atm}	$V_\infty \frac{km}{sec}$
Calc.	100	10^{15}		2.2	3	$5 \cdot 10^7$	$1.3 \cdot 10^3$
	100	10^{14}		1.2	1.4	$7 \cdot 10^6$	$9 \cdot 10^2$
Exp.	100	10^{14}	3	-	~1	$\approx 5 \cdot 10^6$	$\approx 5 \cdot 10^2$
	50	$\ell \cdot 10^{15}$	0.3	-	-	-	$\overline{V} \approx 8 \cdot 10^2$

Figure 13.

of edges. Nonuniformity of illumination is characterized by [text missing]. During target illumination it may be necessary to fulfill the condition that the light emitted by the target should not go to the laser system. For the tetrahedron with N = 4, such variations are possible without broken symmetry. For other polyhedrons with unbroken symmetry, this condition is not fulfilled.

Figures 15 and 16 [missing] illustrate the illumination dependence on the point coordinate along the triangle perimeter and the isometric projection of lines, which is equal to illuminance 4 × 6 × 9 and 20 × 1 × 10 variants.

The calculations for N = 4 tetrahedron correspond to a 216-channel Nd-glass installation named "Delfin" of 10-kJ energy, which is under construction at Lebedev Physical Institute. It is seen that under the condition of converging beams not reaching each other's aperture, the inhomogeneity of illumination may be less than 3%. Without regard for this condition, the inhomogeneity may be less than 1%.

Figure 17 [missing] illustrates the dependences of the illuminance nonuniformity on the defocusing. The reported results indicate that by means of multi-beam installations, one can reduce illumination nonuniformity to 1-3%.

4. In conclusion, we shall report the results of two-dimensional calculations of target compression in the form of thin-walled glass shells. These calculations are performed at the Institute of Applied Mathematics on the basis of a two-dimensional hydrodynamic code and heat conductivity. The calculations are made for the targets and the conditions close to those in the experiments carried out at Lebedev Physical Institute. A study was made of two-dimensional compression of targets with a radius of 70 μ and wall thickness of 4 μ. The energy introduced into the target is of 100 J, and pulse duration is equal to 2 ns. The shape of a spherical shell was assumed to be distorted (see Fig. 18).

Figures 19-23 illustrate the picture of two-dimensional compression for various moments of time for a small initial asymmetry and for large asymmetry. The influence of 2,6,10 harmonics was studied.

From the results obtained, it follows that at the level of initial symmetry of [text missing], the perturbations develop slowly, so the target

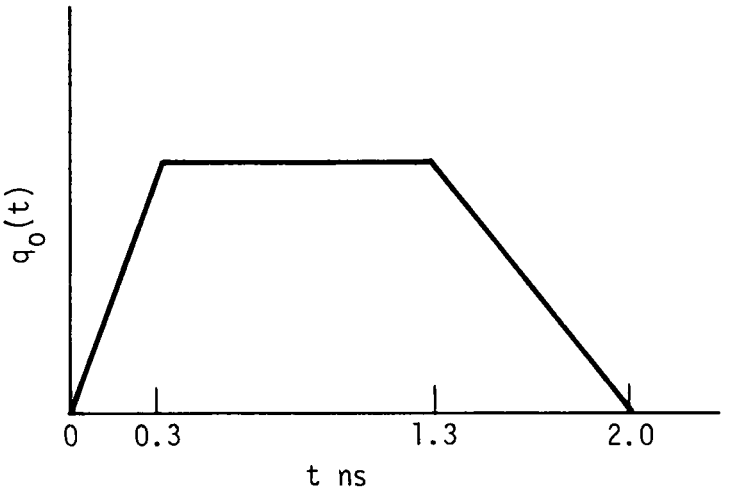
$q_o(t)$
0
0.3
1.3
2.0
t ns

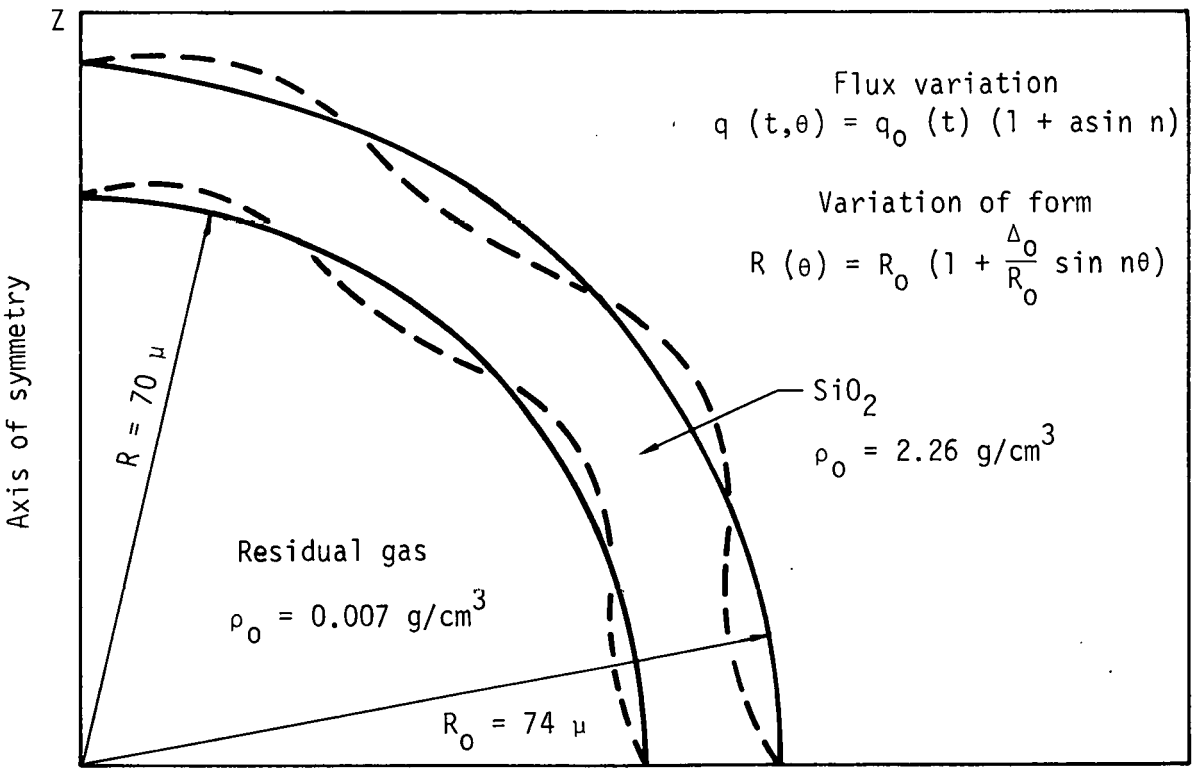
Z
Axis of symmetry
Flux variation
$q\ (t,\theta) = q_o\ (t)\ (1 + a \sin n)$
Variation of form
$R\ (\theta) = R_o\ (1 + \frac{\Delta_o}{R_o} \sin n\theta)$
SiO_2
$\rho_o = 2.26\ g/cm^3$
$R = 70\ \mu$
Residual gas
$\rho_o = 0.007\ g/cm^3$
$R_o = 74\ \mu$

Figure 18.

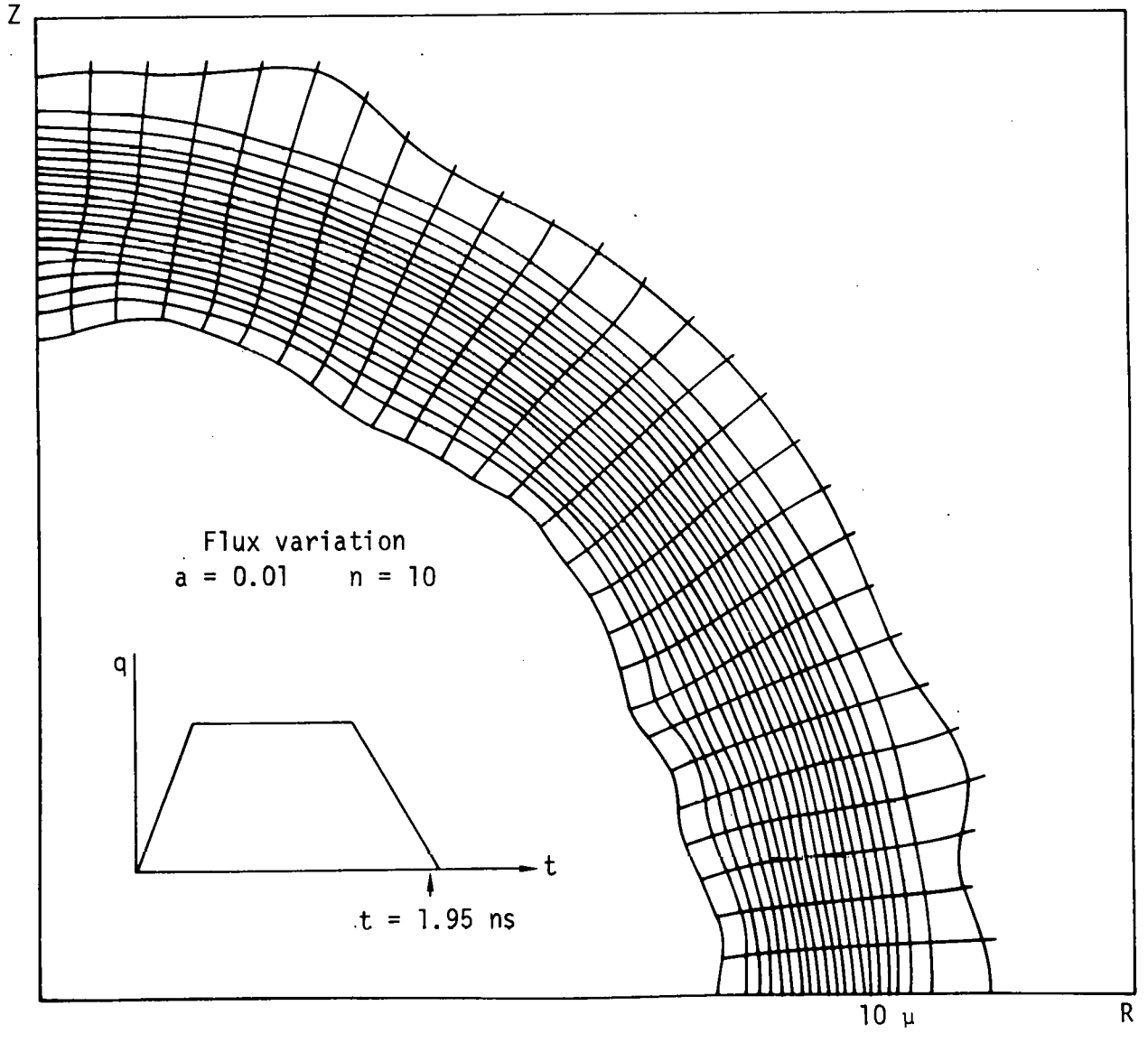

Figure 19.

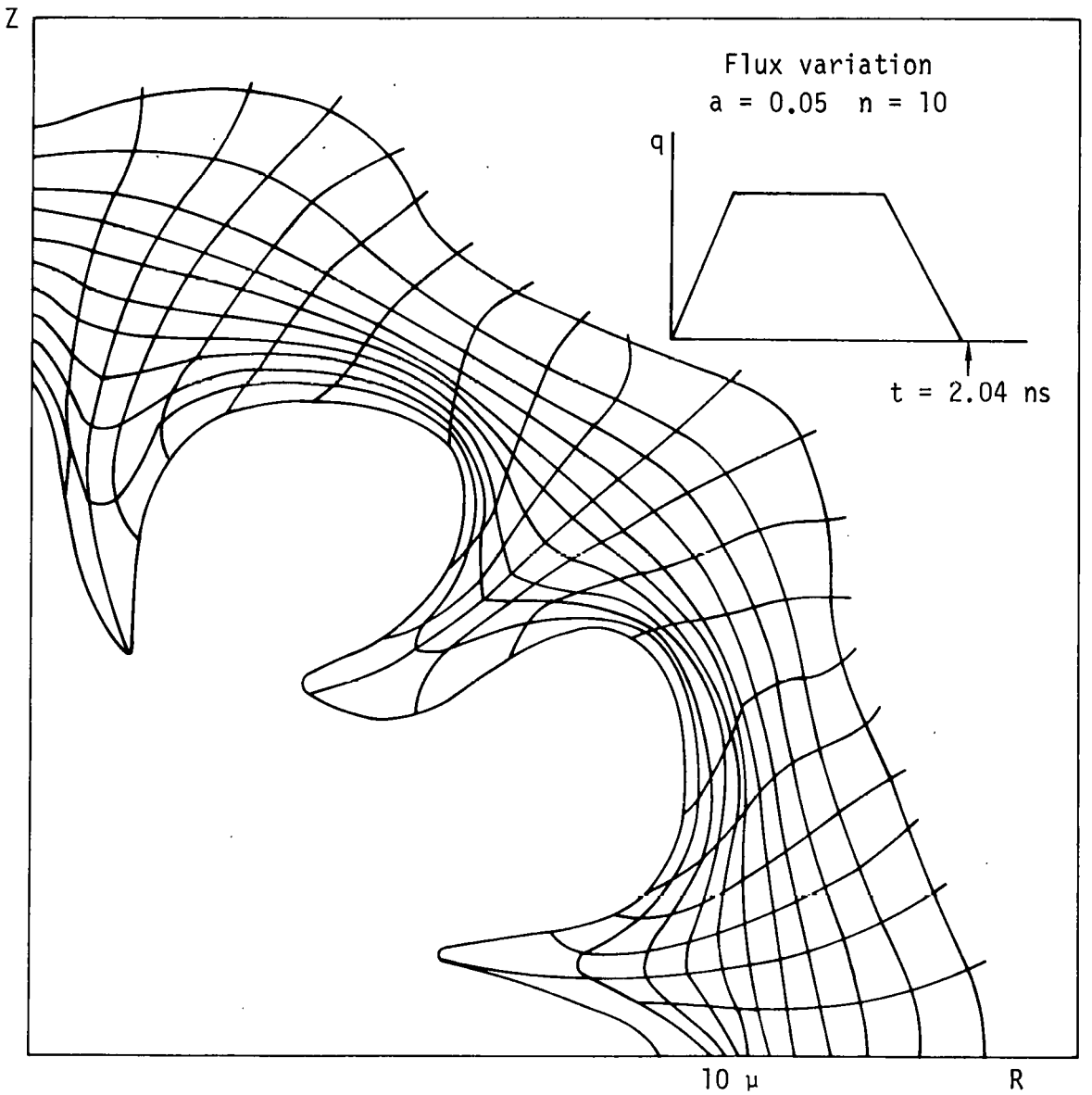

Figure 20.

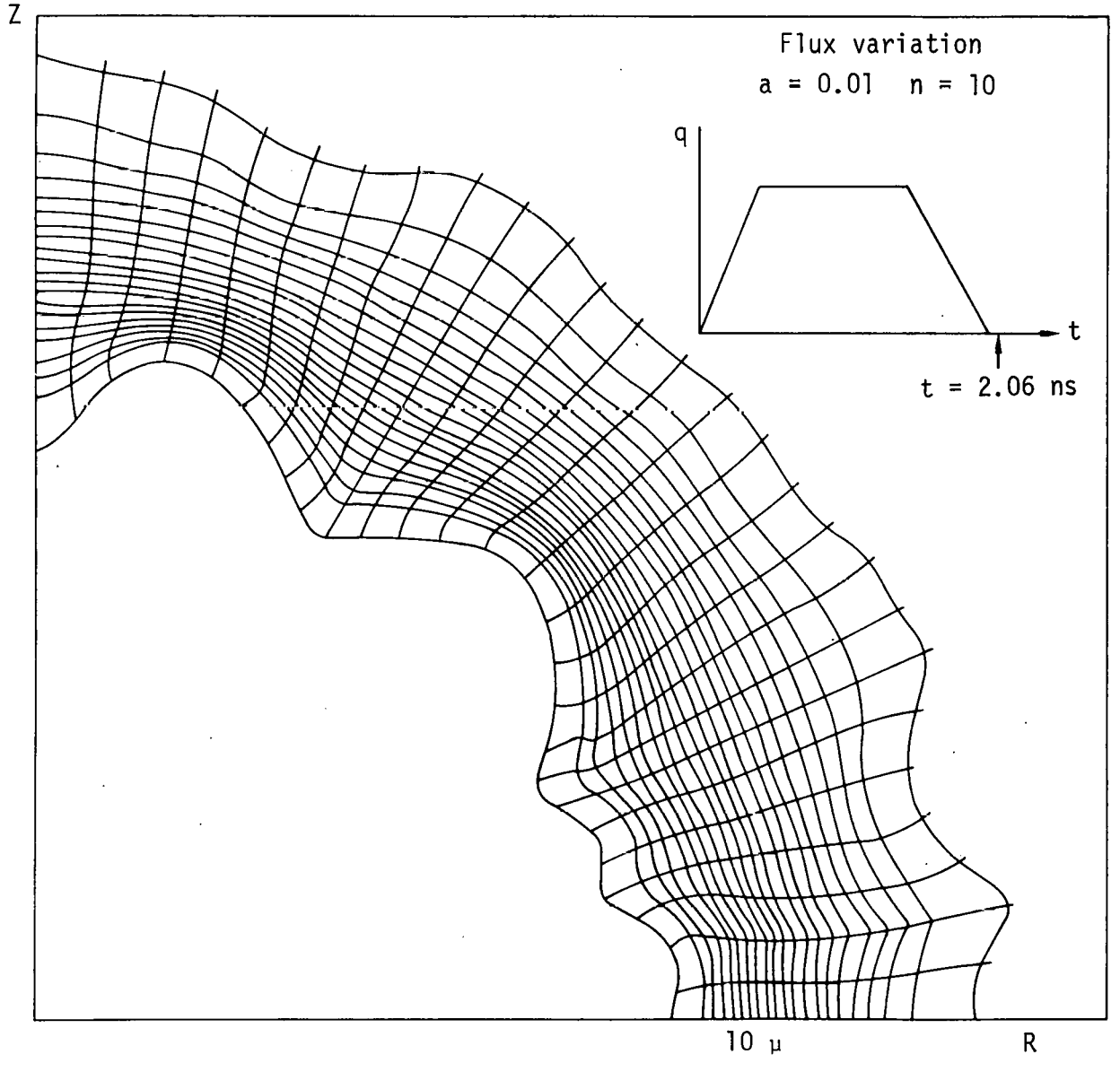

Figure 21.

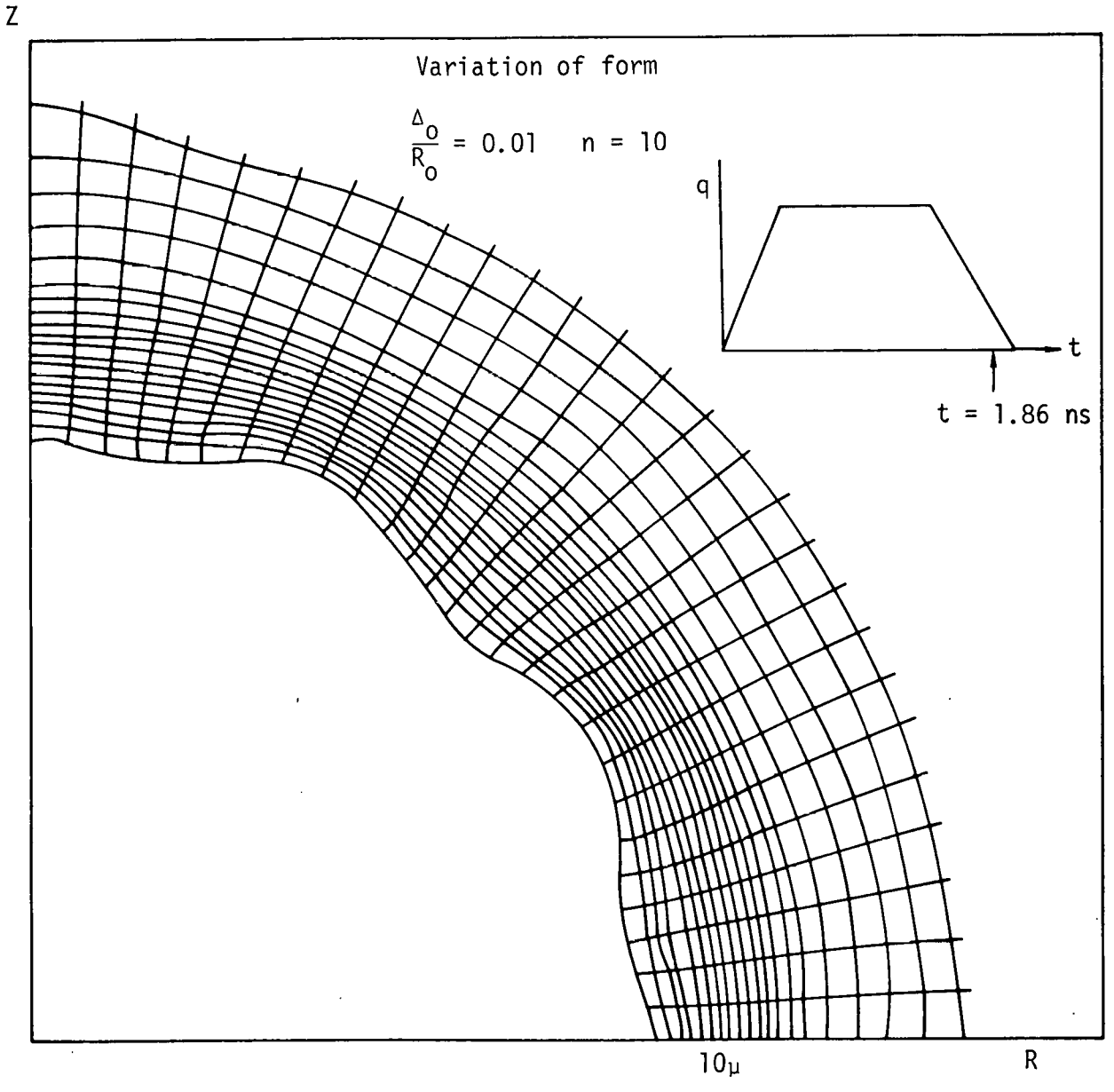

Figure 22.

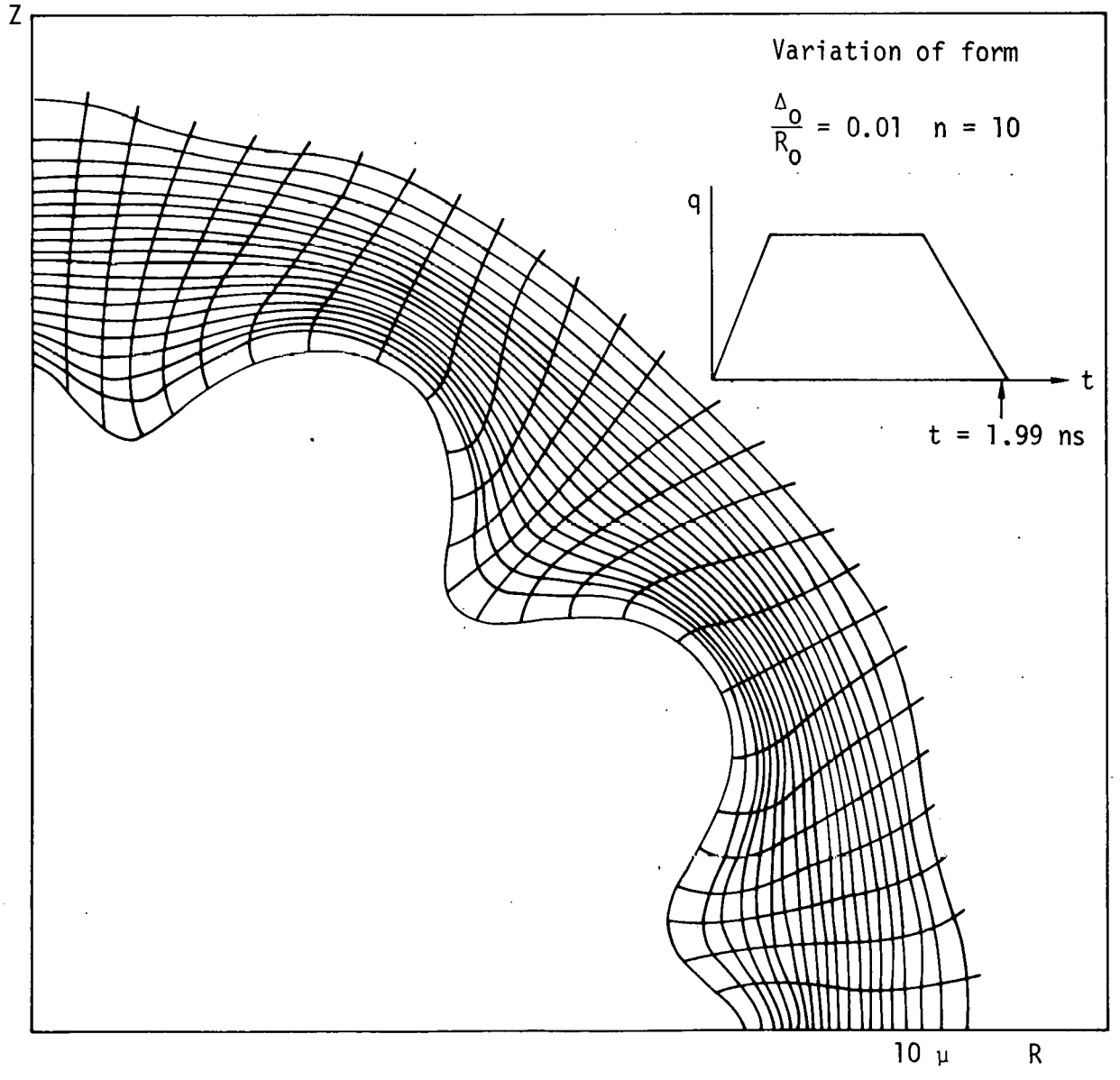

Figure 23.

compression is close to a one-dimensional process. In another calculation, it is found that the inhomogeneity of irradiation is less than the deviations from a spherical shape. Of more influence is the inhomogeneity of the shell thickness. Note that the perturbation develops most powerfully at the final stage of bremsstrahlung.* The linear phase becomes nonlinear at the formation of jets. Under experimental conditions, however, the available deviations from the homogeneity do not prevent us from reaching bulk compression of about 10^3. At such values of compression, the difference of volume-averaged plasma parameters from one-dimensional calculations is negligible. It seems impossible to observe the influence of perturbations with the amplitude $\leq$ 3% from integral measurements (for instance, from obscurograms). Perturbations greater than 10% can lead to significant deviation of the final target shape from spherical.

---

* Perhaps the word "deceleration" is intended. (H.L.S.)

NOTICE

This report was prepared as an account of work sponsored by the United States Government. Neither the United States nor the United States Energy Research & Development Administration, nor any of their employees, nor any of their contractors, subcontractors, or their employees, makes any warranty, express or implied, or assumes any legal liability or responsibility for the accuracy, completeness or usefulness of any information, apparatus, product or process disclosed, or *represents* that its use would not infringe privately-owned rights.

NOTICE

Reference to a company or product name does not imply approval or recommendation of the product by the University of California or the U.S. Energy Research & Development Administration to the exclusion of others that may be suitable.

Printed in the United States of America
Available from
National Technical Information Service
U.S. Department of Commerce
5285 Port Royal Road
Springfield, VA 22161
Price: Printed Copy $; Microfiche $3.00

Page Range	Domestic Price	Page Range	Domestic Price
001–025	$ 3.50	326–350	10.00
026–050	4.00	351–375	10.50
051–075	4.50	376–400	10.75
076–100	5.00	401–425	11.00
101–125	5.50	426–450	11.75
126–150	6.00	451–475	12.00
151–175	6.75	476–500	12.50
176–200	7.50	501–525	12.75
201–225	7.75	526–550	13.00
226–250	8.00	551–575	13.50
251–275	9.00	576–600	13.75
276–300	9.25	601–up	*
301–325	9.75		

*Add $2.50 for each additional 100 page increment from 601 to 1,000 pages; add $4.50 for each additional 100 page increment over 1,000 pages.

WTW/gw/vt/gw

Technical Information Department
LAWRENCE LIVERMORE LABORATORY
University of California | Livermore, California | 94550